Microcrack Network Development in Salt-Rock During Cyclic Loading at Low Confining Pressure

Ding, J., Chester, F. M. and Chester, J. S.
Center for Tectonophysics, Department of Geology and Geophysics, Texas A&M University, College Station, Texas, USA
Shen, X. and Arson, C.
School of Civil and Environmental Engineering, Georgia Institute of Technology, Atlanta, Georgia, USA

ABSTRACT: Triaxial compression tests of synthetic salt-rock are conducted to investigate microfracture development in a semibrittle polycrystalline aggregate. The salt-rock is produced from uniaxial consolidation of granular halite at 150 °C. Following consolidation, the sample is deformed by cyclic loading at room temperature and low confining pressure (Pc = 1 MPa). Load cycles are performed within the elastic regime, up to yielding, and after successive increments of steady ductile flow. At the tested conditions, the samples exhibit ductile behavior with slight work hardening. The microstructure at different stages of deformation indicates that grain-boundary cracking is the dominant brittle deformation mechanism. Microcracking is influenced by the loading configuration and the geometric relationships between neighboring grains. These microcracks display a preferred orientation parallel to the load axis. With cyclic loading, microcracks increase in density and form linked arrays parallel to the direction of loading. As the linked arrays lengthen, grain contacts are progressively opened, which eventually leads to loss of cohesion along surfaces parallel to the loading direction. The observations of crack-network development in salt-rock can improve our understanding of progressive damage and spalling at salt cavern walls.

1. INTRODUCTION

Salt-rock is a viable geomaterial for hydrocarbon storage and waste disposal, because of its favorable creep characteristics and ultra-low permeability for sealing. In the case of storing high-pressure natural gas for balancing seasonal supply, or for pressurized gas associated with wind energy storage, salt caverns are subjected to long-term cyclic loading such that cavern stability becomes a major concern (e.g., Brouard et al., 2012; Minkley et al., 2015). A common stability issue is spalling at salt cavern wall, which not only alters the cavern geometry but also can damage the hanging string and cause roof collapse. Salt block fall due to spalling has been reported in numerous salt caverns, for example the Kiel salt cavern of Germany (Baar, 1977) and the Big Hill cavern of USA (Munson et al., 2004).

Damage development in salt-rock has been studied through field tests (e.g., Cole, 2002; Rokahr et al., 2007), laboratory experiments (e.g., Peach and Spiers, 1996) and numerical simulations (e.g., Zhu and Arson, 2015; Sobolik and Lord, 2015). These studies have provided insights into spalling phenomenon from different perspectives. However, direct observation of fracture initiation and evolution is lacking, and there is a need for additional experimental work to elucidate the mechanisms leading to damage and cavern failure.

To better understand the mechanism of fracture development in semibrittle polycrystalline aggregates, such as exists in salt cavern walls, we conducted cyclic triaxial compression tests on synthetic salt-rock at room temperature and 1 MPa confining pressure. Samples from different stages of cyclic loading were used to prepare thin sections for microstructure characterization. Direct observations of crack damage accumulation were analyzed, and the observed damage mechanisms may provide insight to that associated with spalling in salt caverns. Knowledge gained from this study could be useful to guide numerical modeling of damage development and help design and optimize salt-rock storage facilities.

2. EXPERIMENTAL METHODS

2.1. Synthetic salt-rock sample

The synthetic salt-rock sample used in this study is fabricated through uniaxial consolidation of reagent-grade granular halite at the following conditions:

- Grain size ranges between 0.3 – 0.355 mm;

- Consolidation temperature is 150 °C;
- Maximum axial stress is 75 MPa;
- Displacement rate is 0.034 mm/s.

Ding et al. (2016) described in detail the sample fabrication process and microstructure characteristics. Bulk porosity of the synthetic salt-rock sample produced from the above conditions is around 6%. The sample was kept dry throughout all stages of this study.

2.2. Cyclic triaxial compression test

The cylindrical, synthetic salt-rock samples produced through consolidation were first wrapped with silver foil that was annealed at 700 °C. Then the sample was preloaded in a triaxial apparatus under 60 MPa isostatic pressure for half an hour. This preloading step not only avoids significant consolidation during cyclic loading test, but also allows soft silver jacket to fully bond to the sample. Then two rosette strain gauges 6.35 mm gauge length) were glued onto the silver foil at the middle of the sample (Fig. 1). These two strain gauges were positioned at opposing sides of the sample, so that axial and radial strain measurements could be averaged to account for sample tilting. A total of eight unloading-reloading cycles were employed, in addition to initial loading and final unloading. One unloading-reloading cycle was applied in the elastic deformation regime, while the rest load cycles were fulfilled after plastic yielding.
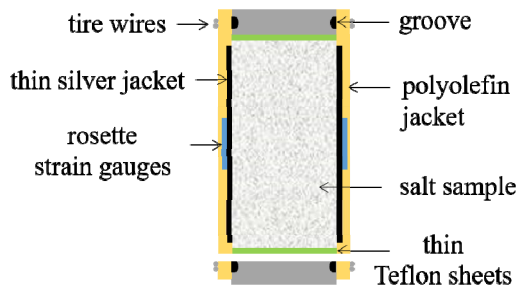

Fig. 1. Schematic of sample instrumentation for cyclic triaxial compression tests

2.3. Microstructure characterization using optical microscopy

Using repeat experiments, synthetic salt-rock samples before, during, and at the end of cyclic loading were extracted for microstructure observation. These samples were epoxy-saturated, cut, and polished to make petrographic sections, and then chemically etched to allow observation of grain-scale features, including grain boundaries and microcracks. The sectioning and etching procedures follow the techniques developed by Spiers et al. (1986) with only minor modifications. Thin section images were taken from the center portion of the sample using 20x magnification, and stitched together to allow

observation of more than 100 grains. On the stitched image, salt grain boundaries were traced and opening-mode microcracks were interpreted based on the following two criteria:

(i) There is clear separation between two salt grain boundaries;
(ii) The opposing sides of these two salt grain boundaries match well geometrically, which indicates there were previously in contact.

3. EXPERIMENTAL RESULTS

3.1. Mechanical behavior

At room temperature and 1 MPa confining pressure, synthetic salt-rock exhibits ductile behavior (Fig. 2). The first unloading-reloading cycle nearly fully overly the initial loading curve, which indicates dominant elastic behavior. After yielding, the sample deforms plastically with slight work hardening. Each unloading is applied to zero differential stress; subsequent reloading does not produce significant hysteresis. Volumetric strain is determined from axial and radial strain measurements. The sample behavior first shows slight compaction (positive volumetric strain), followed by continuous dilation (negative volumetric strain). At the end of the test, the sample increases in volume by about 2.6%.
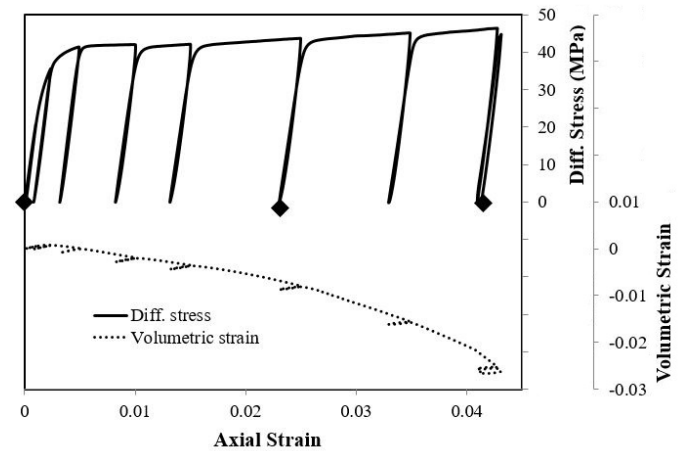

Fig. 2. Differential stress and volumetric strain versus axial strain; negative volumetric strain indicates dilation, diamonds show where samples are made into thin sections.

3.2. Microstructure

The synthetic salt-rock produced from uniaxial consolidation at elevated temperature shows minor intragranular microcracking (Fig. 3a). Almost all of these intragranular microcracks are associated with fluid inclusions present in salt grains. These fluid inclusions act as stress concentrators and promote microcracking. There is no evidence for separation at grain contacts as all of them are tight, which results from crystal-plastic deformation of salt grains (Ding et al., 2016). After
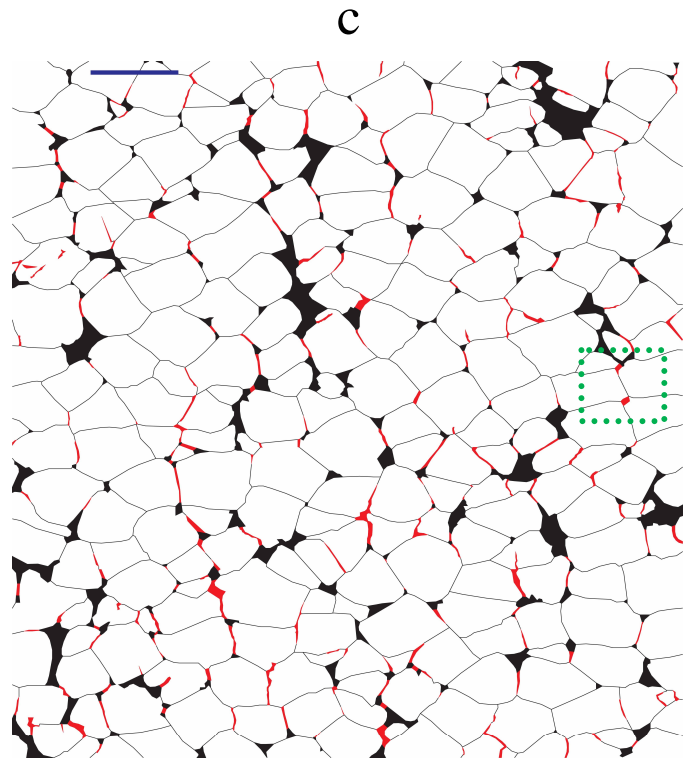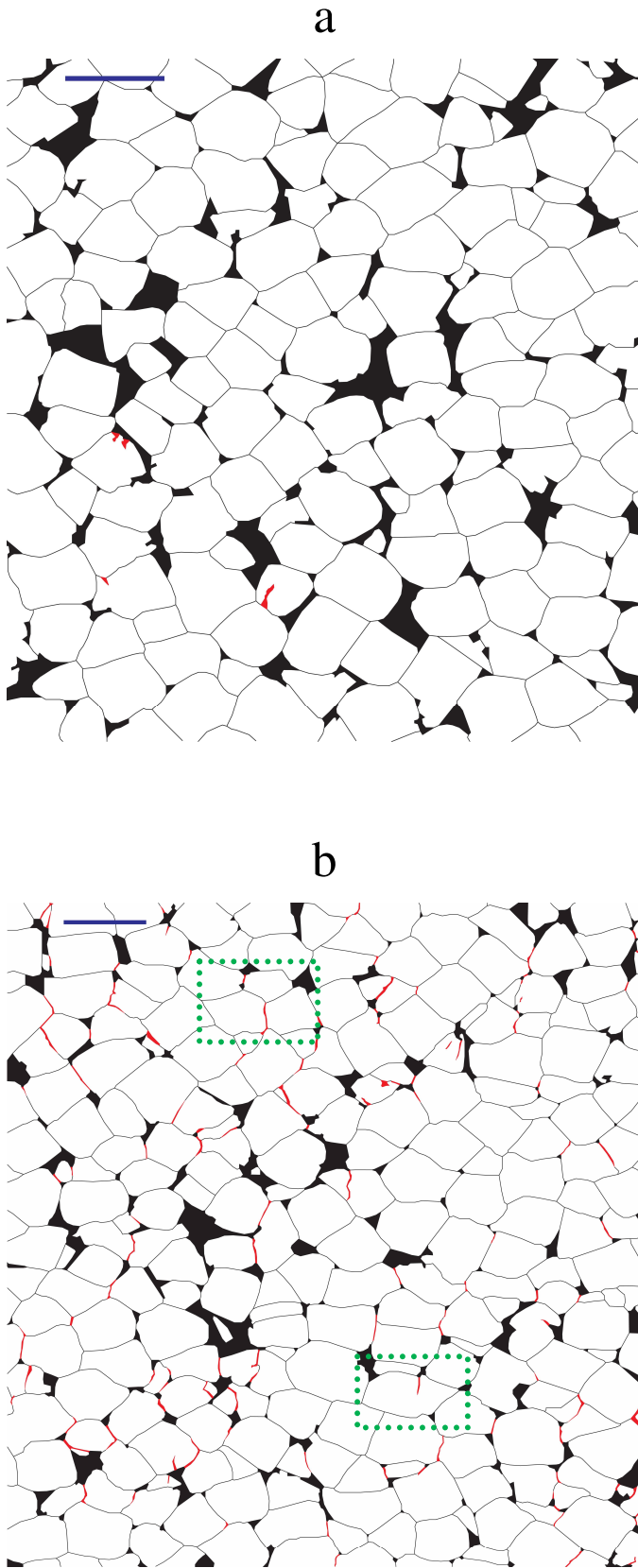
a

c

Fig. 3. Line tracings of micrographs of salt grains (white), pores (black) and opening-mode microcracks (red) of synthetic salt-rock with (a) axial strain = 0; (b) axial strain = 2.4%; (c) axial strain = 4.3%; axial stress is vertical, dark blue scale bar represents 0.5 mm; images are taken at sample center; note all grain contacts are tight when axial strain is zero; dashed squares show locations corresponding to crack geometries shown in Fig. 4.
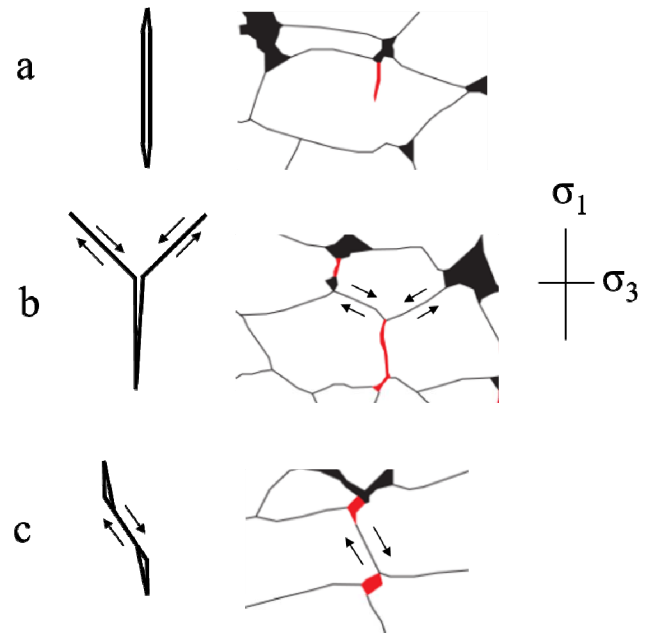
b

Fig. 4. Three microcracking modes discussed by Brace et al. (1966) and corresponding examples from synthetic salt-rock microstructures; σ_1 and σ_3 are maximum and minimum principal stresses, respectively.

cyclic triaxial loading to an axial strain of 2.4%, grain-boundary cracking becomes the dominant brittle deformation mechanism (Fig. 3b). These microcracks exhibit a preferred orientation that is sub-parallel to the axial loading direction. With further cyclic loading, dilatant grain-boundary microcracks increase in density as well as in separation, as documented at an axial strain of 4.3% (Fig. 3c). These grain-boundary microcracks also display a clear tendency to link with neighboring cracks in the axial direction.

4. DISCUSSION

4.1. Cracking mode

At the tested conditions, grain-boundary microcracking is the dominant brittle deformation mechanism and leads to pronounced dilation. The grain-boundary microcracking is influenced by loading configuration and geometric relationships between neighboring grains. Brace et al. (1966) discussed three basic modes of microcracking that are all observed in the microstructure of our deformed synthetic salt-rock. The isolated axial cracks occur mostly within salt grains that form in association with preexisting fluid inclusions (Fig. 4a). This type of microcrack is rare as fluid inclusions in the sample are few. At grain triple-junctions, the vertical grain contact (parallel to the load axis) may be popped open as a result of shearing along the other two boundaries (Fig. 4b). When grain contacts are oriented inclined with respect to load axis, sliding may occur and leads to opening-mode cracks at two ends, forming wing-crack (Fig. 4c). The latter two cracking modes are dominant and cause damage to grain boundaries. Since salt-rock deforms plastically at the same time, crack opening is also accommodated by creeping at salt grain contacts, in addition to shearing.

4.2. Preferred orientation

The opening-mode microcracks are fitted to ellipses using ImageJ image analysis software and the angle between the major axis and the direction perpendicular to the load axis is plotted in rose diagrams (Fig. 5). At different axial strains, both samples show a preferred orientation with the major axis sup-parallel to the load axis. As axial strain increases from 2.4% to 4.3%, microcrack orientation becomes more uniform with respect to the load axis.

4.3. Microcrack linking

Opening-mode microcracks are analyzed to reveal the degree of linking with increasing deformation. Microcracks are considered linked if they connect to the same void or to a single grain contact segment oriented consistent with shear motion. It is apparent that increasing cyclic loading and deformation leads to linking between microcracks (Fig. 6). In the 4.3% axial strain sample, many microcracks link into long arrays in

the direction of load axis, and the percentage of more than four linked microcracks is almost three times as in the 2.4% axial strain sample. As microcracks link, the lateral (in the direction normal to the load axis) integrity of the sample is progressively decreased.

a

b

Fig. 5. Rose diagrams of opening-mode microcrack orientation for synthetic salt-rock with (a) axial strain = 2.4%; (b) axial strain = 4.3%; the angle is between the major axis of the best fit ellipse of the microcrack and the direction perpendicular to load axis (90° is in the direction of axial stress).
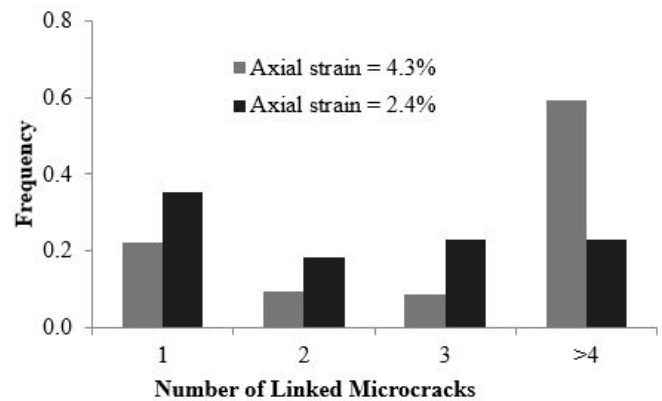

Fig. 6. Histogram of the frequency of linked microcrack arrays versus the number of microcracks linked.

Microcrack linking is more severe at sample boundaries, since it is close to the free interface between the sample and the confining fluid (Fig. 7). Nearly all inclined grain contacts are open or partially open, but the boundaries at high-angles to the load axis remain tight. Thus, linkage of microcracks in the vertical arrays essentially producing pillars that support the axial load. The observation here may be analogous to the state that

precedes spalling along the free surface (if no sample jacket was present). Further disturbance of the grain contacts by cyclic loading would cause sample to lose cohesion completely.

4.4. Implications to gas storage salt cavern

In the gas storage salt caverns where wall is subject to cyclic loading, our experimental observations suggest the following mechanism for spalling. Cyclic loading at low confining pressure and temperature causes progressive microcracking at salt grain contacts. These contacts are prone to open mainly through popping by a third grain or shearing along inclined grain boundaries. These opening-mode microcracks preferentially form parallel to the load axis. As damage accumulates, they link to form arrays. As the linked arrays increase in length and number, larger networks may form leading to complete loss of cohesion and spalling.

In this study, the synthetic samples have pores contributing greater porosity than likely occurs in natural salt-rocks. For polycrystalline aggregates that are less porous than our synthetic salt-rock samples, grain-boundary shearing and opening mode microcracking would still likely occur and link to form similar arrays. In these cases, less axial strain may be necessary to achieve spalling; future work should test this hypothesis.
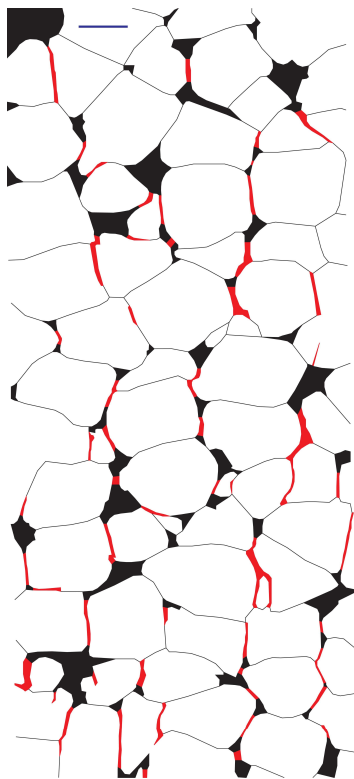

Fig. 7. Line tracing from micrographs of salt grains (white), pores (black) and opening-mode microcracks (red) of synthetic salt-rock sample with axial strain = 4.3%; axial stress is vertical, dark blue scale bar represents 0.2 mm, images are taken close to sample boundary; the sample-fluid interface is vertical on the right side of the map.

5. CONCLUSIONS

In this study, we conducted cyclic triaxial compression experiments on synthetic salt-rock samples to investigate microcrack and damage accumulation at low confining pressure in semibrittle polycrystalline aggregates. Mechanical behavior and microstructure observations demonstrate the following:

(i) At room temperature and low confining pressure, grain-boundary microcracking is the dominant brittle deformation mechanism.

(ii) Grain-boundary microcracks develop preferably in the loading direction and tend to link with increasing deformation.

(iii) Cyclic loading leads to progressive lengthening of linked crack arrays, which is an import mechanism of damage development that ultimately could lead to spalling at salt cavern walls.

REFERENCES

1. Baar, C. A. 1977. *Applied salt-rock mechanics 1: the in-situ behavior of salt rocks*. 1st ed. Amsterdam: Elsevier Science.

2. Brace, W. F., B. W. Paulding, and C. H. Scholz. 1966. Dilatancy in the fracture of crystalline rocks. *J. Geophys. Res.* 71(16), 3,939-3,953.

3. Brouard, B., P. Berest, H. Djizanne, and A. Frangi. 2012. Mechanical stability of a salt cavern submitted to high-frequency cycles. In *Proceedings of the Seventh Conference on the Mechanical Behavior of Salt, Paris 16-19 April 2012,* eds. P. Bérest et al., 381-390. London: Taylor & Francis.

4. Cole, R. 2002. The long term effects of high pressure natural gas storage on salt caverns. In *Proceedings of SMRI Spring Meeting, Banff, 28 April - 1 May 2002,* 75–97.

5. Ding, J., F. M. Chester, J. S. Chester, C. Zhu, and C. Arson. 2016. Mechanical behavior and microstructure development in consolidation of nominally dry granular salt. In *Proceedings of Fiftieth US Rock Mechanics/Geomechanics Symposium, Houston, 26-29 June 2016.*

6. Minkley, W., M. Knauth, T. Fabig, and N. Farag. 2015. Stability and integrity of salt caverns under consideration of hydro-mechanical loading. In *Proceedings of the Seventh Conference on the Mechanical Behavior of Salt, Paris 16-19 April 2012,*

eds. P. Bérest et al., 217-227. London: Taylor & Francis.

7. Munson, D.E., B. Ehgartner, S. Bauer, C. Rautman, and R. Myers. 2004. Analysis of a salt fall in Big Hill Cavern 103, and a preliminary concept of salt dome structure. In *Proceedings of SMRI Spring Meeting, Wichita, 18 - 21 April 2004*, 57–72.

8. Peach, C.J., and C.J. Spiers. 1996. Influence of crystal plastic deformation on dilatancy and permeability development in synthetic salt rock. *Tectonophysics*, 256(1): 101-128.

9. Rokahr, R., K. Staudtmeister, D. Zander-Schiebenhöfer, and J. I. Johansen. 2007. In-situ test with a gas storage cavern as a basis for optimization. In *Proceedings of SMRI Spring Meeting, Basel, 29 April - 2 May 2007,* 84–97.

10. Sobolik, S. R., and A. S. Lord. 2015. Operation maintenance and monitoring of large-diameter caverns in oil storage facilities in domal salt. In *Proceedings of the Eighth Conference on the Mechanical Behavior of Salt, Rapid city, 26-18 May 2015,* eds. L. Roberts et al., 229-241. London: Taylor & Francis.

11. Spiers, C.J., J.L. Urai, G.S. Lister, J.N. Boland, and H.J.Zwart. 1986. *The influence of fluid-rock interaction onthe rheology of salt rock.* 1st ed. Luxembourg: Commission of the European Communities.

12. Zhu, C., and C. Arson. 2015. Fabric-based modeling of thermo-mechanical damage and healing around salt caverns. In *Proceedings of the Eighth Conference on the Mechanical Behavior of Salt, Rapid city, 26-18 May 2015,* eds. L. Roberts et al., 243-253. London: Taylor & Francis.